Research article

Single shot all-optical switching in amorphous TbCo and the role of element specific damping on helicity-independent all-optical switching

Syam Prasad P., Jyoti Ranjan Mohanty *

Nanomagnetism and Microscopy Laboratory, Department of Physics, Indian Institute of Technology Hyderabad, Kandi, Sangareddy, 502284, Telangana, India

ABSTRACT

After the discovery of helicity-independent all-optical switching (HI-AOS)in amorphous GdFeCo using femtosecond laser pulse, significant efforts are made to understand the underlying mechanism in HI-AOS and also to utilize this phenomenon for ultra-high density data storage applications. HI-AOS has predominantly been observed in Gd-based ferrimagnetic alloys such as GdFeCo, GdCo, GdFe, etc. Efforts are required to extend the range of material which shows HI-AOS. With the help of atomistic spin dynamics calculations combined with two temperature model, we demonstrate the single-shot helicity-independent all-optical switching in amorphous Tb_xCo_{100-x} ferrimagnet using femtosecond laser pulses. The value of x is varied from $x = 18\%$ to $x = 36\%$, and a deterministic HI-AOS is observed for the composition range $x = 20\%$ to $x = 32\%$. The threshold input laser energy is found to decrease with an increase in Tb concentration. Understanding the role of the damping parameter is crucial to understand the different coupling mechanism that governs HI-AOS. Further, an element specific damping is applied to both sublattices, and the damping constant of the Tb sublattice is kept at 0.05 while that of the Co sublattice is varied from 0.005 to 0.05. The results show the damping constant strongly influences the HI-AOS, and the higher damping constant is crucial for the HI-AOS.

1. Introduction

Manipulating the magnetization at picosecond and sub-picosecond timescale got immense attention after the realization of ultrafast demagnetization in Ni using the femtosecond laser pulses [1]. This discovery stimulated an intense area of research known as ultrafast magnetization dynamics. Since the first experimental realization of ultrafast demagnetization in Ni, extensive research has focused on understanding the underlying mechanism behind the ultrafast demagnetization and also utilizing this property for future data storage applications [2–6]. In 2007, Stanciu et al. showed the optical switching in amorphous GdFeCo thin film using circularly polarised femtosecond laser pulses [4]. This breakthrough experiment sparked a discussion over the source of ultrafast all-optical switching, and the observed switching was attributed to the inverse Faraday effect (IFE) [4,7,8]. Since the final magnetization state is decided by the helicity of the laser pulse used, it is named as helicity dependent all-optical switching (HD-AOS). Further research in AOS revealed that a linearly polarised laser pulse also could stimulate a deterministic magnetization reversal, which is known as helicity independent all-optical switching (HI-AOS). In 2012, Ostler et al. reported the first experimental observation of HI-AOS [9]. Since the ultrafast heating generated by the ultrashort laser pulse act

as a key driving force to the HI-AOS is also referred to as thermally induced magnetization switching (TIMS).

The HI-AOS has been the subject of many experimental, as well as theoretical studies [9–18]. The HI-AOS is commonly observed in Gd based RE-TM alloys and multilayers systems, including GdCo [11], GdFeCo [9,10], Pt/Co/Gd [12], Co/Pt/Co/GdFeCo [13], while Tb based systems have shown limited success in HI-AOS. But HD-AOS is predominantly observed in Tb based systems [19,20]. Single shot HI-AOS is observed in electrodes of atomically thin multilayers of Tb/Co [21]; it is also reported in amorphous TbFeCo by employing a pair of plasmonic antennas, which enhance the optical field [22]. A Ceballos et al. have reported single shot HI-AOS in amorphous GdTbCo by varying Tb concentration while $Tb_{22}Co_{78}$ has only shown thermal demagnetization [23]. The role of magnetization compensation temperature (T_M) in HI-AOS has been a subject of debate since the discovery of HI-AOS in disordered RE-TM ferrimagnetic alloys, and it is believed that heating the sample through compensation temperature is pivotal for HI-AOS [4]. Later it was verified that heating the sample through T_M is not essential for HI-AOS [9]. R. Moreno et al. investigated the role T_M and pulse duration in HI-AOS using atomistic spin dynamics (ASD) modelling in amorphous TbCo [24]. It has been found that the occurrence of T_M is not necessary for HI-AOS to observe, and HI-AOS

---

occurs for the laser pulses having pulse widths comparable to the time scales of exchange energy.

In the present investigation, we aim to predict the possibility of HI-AOS in amorphous TbCo using atomistic spin dynamics and hence to find the range of parameters it can show a deterministic optical switching. Since ferrimagnetic alloys with non-equivalent sublattices are crucial for HI-AOS, RE-TM alloys are potential candidates for HI-AOS. High magnetic anisotropy materials are required to maintain the high signal to noise ratio(SNR) and thermal stability to implement optical writing in magnetic memories. The amorphous TbCo has been found interesting because of its high uniaxial anisotropy, making it suitable for data storage applications. Here we investigate the HI-AOS in Tb_xCo_{100-x}(x is varied from 18 to 36) for a wide range of fluence values. Further, it is essential to have knowledge of the role of energy transfers and coupling mechanisms between different heat baths to understand and control the HI-AOS. The studies [11,23,25] show that the spin-electron and spin-lattice couplings have a strong influence on HI-AOS. In this context, elucidating the role of phenomenological damping is crucial to understand the role of the electron-spin coupling mechanism and energy transfers between different heat baths that govern HI-AOS [26–28]. For this purpose, element-specific damping is applied to both sublattices, with the damping constant of Tb kept at a constant value of 0.05, while that of Co is varied from 0.005 to 0.05

2. Atomistic spin dynamics modelling

We use atomistic spin dynamics (ASD) simulations coupled with two temperature model (2TM) to study the ultrafast laser induced spin dynamics in amorphous TbCo. To model the amorphous TbCo, first, we constructed an fcc lattice with specified dimensions. To mimic the disordered nature of amorphous TbCo, randomly chosen Co sites are replaced with Tb atoms. Here the simulated system contains $56 \times 56 \times 28$ fcc cells with periodic boundary conditions in x and y directions. The energetics of each site is characterised by the Heisenberg Hamiltonian, defined by [29]

$$\mathcal{H} = -\sum_{i>j} J_{ij}\mathbf{S}_i \cdot \mathbf{S}_j - \sum_i k_u S_z^2 \tag{1}$$

where $\mathbf{S}_i$ is the unit vector associated with the localised spin moment at site i, J_{ij} denotes the exchange coupling between sites i and j, and k_u represents the onsite uniaxial anisotropy constant. The stochastic Landau–Lifshitz–Gilbert(s-LLG) equation is used to predict the temporal evolution of the spin system.

$$\frac{d\mathbf{S}_i}{dt} = -\frac{\gamma_i}{(1+\lambda_i^2)\mu_i}\mathbf{S}_i \times [\mathbf{H}_i + \lambda_i \mathbf{S}_i \times \mathbf{H}_i] \tag{2}$$

where γ_i is the gyromagnetic ratio, and λ_i is the phenomenological damping constant. μ_i represents the magnetic moment, and $\mathbf{H}_i = -\frac{\partial \mathcal{H}}{\partial \mathbf{S}_i} + \zeta_i$ denotes the effective field at each site including the stochastic thermal field ζ_i. The phenomenological damping constant λ_i couples ζ_i to the electron temperature(T_e).

To parametrise the spin Hamiltonian, the following values are used. The Co and Tb magnetic moments are set as $\mu_{Co} = 1.61\mu_B$ [30] and $\mu_{Tb} = 9.34\mu_B$ [31], which corresponds to bulk magnetization values of Co and Tb. These values will not change significantly when they are alloyed [30,32]. To produce the macroscopic anisotropy variation with composition, different anisotropy constants are assigned to both Co and Tb sublattices. In this study, the onsite anisotropy values used are $k_u(Co) = 3.73 \times 10^{-23}$ J/atom $k_u(Tb) = 2.16 \times 10^{-22}$ J/atom respectively [24]. Initially, a damping constant of 0.05 is applied to both sublattices, and later damping constant of Co is varied from 0.005 to 0.05 while that of Tb is kept constant at 0.05 to study the role of element-specific damping. The exchange parameters of Tb and Co are calculated from bulk Curie Temperatures (T_c) values [33,34]. An antiferromagnetic coupling of -1×10^{-21} J/link is used as intersublattice coupling constant, which will give the experimentally observed T_M

Table 1
List of exchange parameters used for TbCo [24].

Type of exchange interaction	Value (J/link)
J_{Co-Co}^{bulk}	5.9×10^{-21}
J_{Tb-Tb}^{bulk}	8.2×10^{-22}
J_{Co-Tb}	-1.0×10^{-21}
$J_{Co-Tb-Co}$	-4.4×10^{-21}

values [24]. Experimentally observed T_c values suggest an effective decrease in the exchange parameter at Co sites as Tb concentration increases [35,36]. This is accounted for in the model by considering an additional antiferromagnetic exchange at Co sites that arises in the vicinity of Tb. The effective exchange parameter at the Co site is calculated as follows [24].

$$J_{Co-Co}^{eff} = J_{Co-Co}^{bulk} + J_{Co-Tb-Co}\frac{x}{1-x} \tag{3}$$

The decrease in J_{Co-Co}^{eff} is found to be proportionate with the concentration of Tb x. The exchange parameters for TbCo are listed in Table 1.

The two temperature model (2TM) combined with ASD simulations is used to determine laser induced time dynamics of electron and phonon temperatures. The coupled equations for 2TM are as follows

$$C_e\frac{dT_e(t)}{dt} = -G_{ep}[T_e(t) - T_{ph}(t)] + P(t)$$
$$C_{ph}\frac{dT_{ph}(t)}{dt} = -G_{ep}[T_{ph}(t) - T_e(t)] \tag{4}$$
$$P(t) = P_0 e^{-(t/\tau_p)^2}$$

where T_e and T_{ph} are electron and phonon temperatures, $C_e = \gamma T_e$ and C_{ph} represents their respective heat capacities, and G_{ep} stands for the coupling between electron and phonon heat baths. $P(t)$ is the input laser energy absorbed by the electrons, and it is represented by a Gaussian profile with a laser pulse width τ_p. The 2TM parameters used here are the values of amorphous $TbFe_2$ taken from Ref. [37]. We assume that these values are constant over the composition range considered here. The parameters used here are $\gamma = 2.20 \times 10^2$ Jm^{-3} K^{-2}, $C_{ph} = 2.3 \times 10^6$ Jm^{-3} K^{-1}, and $G_{ep} = 6.6 \times 10^{17}$ Js^{-1} m^{-3} K^{-1} respectively. All the simulations are carried out at 300 K using the *vampire* [29] atomistic simulation package.

3. Results and discussion

3.1. Single shot helicity-independent all-optical switching in amorphous Tb_xCo_{100-x} alloys

First, we investigate the possibility of HI-AOS in amorphous TbCo by irradiating a 50 fs laser pulse at a wide range of fluence values. Fig. 1 shows the element-specific magnetization dynamics and electron-phonon temperature profile of $Tb_{26}Co_{74}$ during the laser heating at a fluence value of 28 mJ/cm^2. When the system is irradiated with a laser pulse, electrons quickly absorb energy from the laser. In the first 300 fs, the electron thermalisation happens, and electron temperature(T_e) reaches a maximum value of around 1500 K. However, the exact role of temperature is unknown in HI-AOS; the T_e needs to rapidly overcome the T_c to decouple the strong exchange field, which is responsible for the antiferromagnetic alignment between Tb and Co sublattices. As a result, both Tb and Co sublattices demagnetize individually at a different demagnetization rate. Co demagnetizes at a faster rate, while Tb does at a slower rate [9]. In elemental ferromagnets, the demagnetization time is proportional to $\mu/\lambda T_e$, where μ, λ, and T_e are the magnetic moment, damping constant and electron temperature, respectively [26]. Here Co demagnetizes at 1.08 ps whereas Tb demagnetizes at 1.28 ps. After reaching the maximum T_e, the heat is transferred from electrons to phonons till reaching the equilibrium
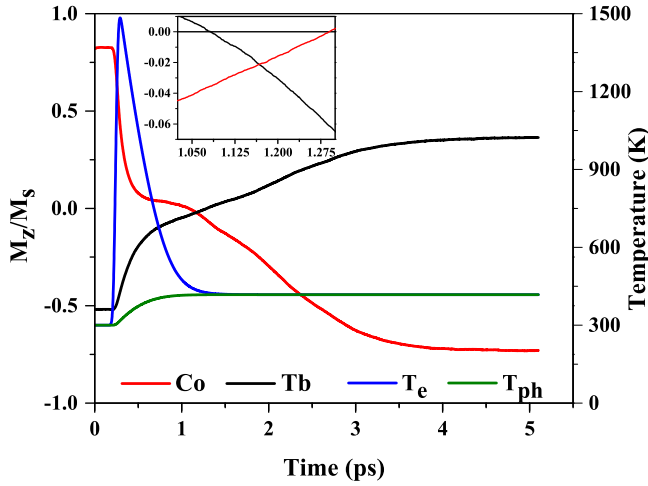
Fig. 1. Element specific magnetization dynamics and electron-phonon temperature profile of $Tb_{26}Co_{74}$ during the laser heating by a 50 fs laser pulse at a fluence of 28 mJ/cm². Red and Black lines represent Co and Tb magnetization, respectively. The reduced magnetization M_z/M_s is the z component of the magnetization of each sublattice divided by the magnetization of that sublattice at 0 K. The blue and green lines represent electron and phonon temperatures, respectively. The inset shows the enlarged view of the transient ferromagnetic like state (TFLS) where the Tb and Co moments align parallel temporarily during HI-AOS.
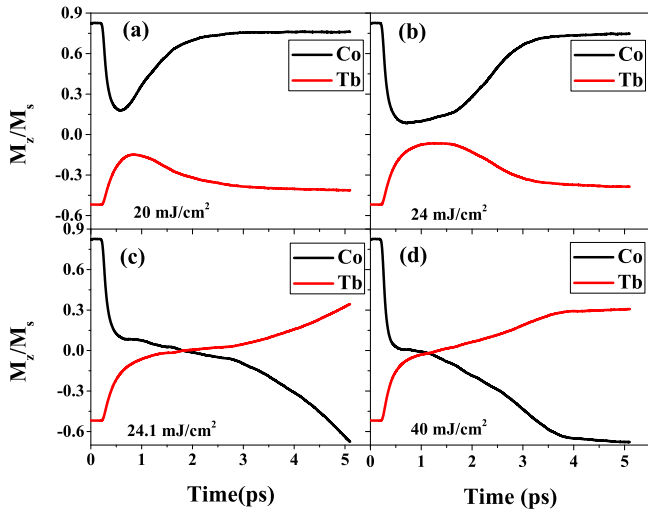

Fig. 2. Element specific magnetization dynamics of $Tb_{26}Co_{74}$ at 4 different fluences; *(a)* 20 mJ/cm², *(b)* 24 mJ/cm², *(c)* 24.1 mJ/cm², and *(d)* 40 mJ/cm². Black and Red lines represent Co and Tb magnetization, respectively.

temperature, and the electron–phonon equilibration happens around 1.3 ps. During this process, the completely demagnetised Co sublattice starts to remagnetize towards the equilibrium magnetization, while Tb continues to demagnetize towards the equilibrium magnetization(at T_e). The conservation of angular momentum results in the reversal of Co moments and forms a transient ferromagnetic like state (TFLS) in which Co and Tb moments temporarily align parallel. Further cooling restores the strong antiferromagnetic coupling, which drives the Tb moments in the opposite direction. The observed duration of TFLS here is low (300 fs) compared to that in GdFeCo (1 ps) [10].

Fig. 2 shows the element-specific magnetization dynamics of $Tb_{26}Co_{74}$ at 4 different fluence values; 20 mJ/cm², 24 mJ/cm², 24.1 mJ/cm², and 40 mJ/cm². Here we observe an optical switching when the fluence value reaches a threshold of 24.1 mJ/cm². Similarly, we have investigated the possibility of HI-AOS in different compositions of Tb_xCo_{100-x}, where *x* ranges from 18% to 36%. A deterministic HI-AOS
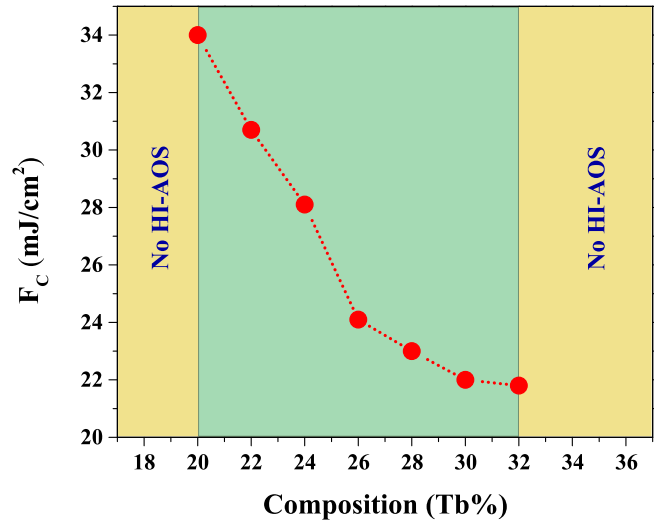

Fig. 3. The variation of critical fluence with Tb concentration. The regions coloured green represent compositions with no HI-AOS.

is observed for the range x = 20% to x = 32%; no HI-AOS is observed for the compositions $Tb_{18}Co_{82}$, $Tb_{34}Co_{66}$, and $Tb_{36}Co_{64}$. There exist no compensation temperature(T_M) for $Tb_{34}Co_{66}$ and $Tb_{36}Co_{64}$, and that of $Tb_{18}Co_{82}$ is below room temperature. Initially, it is believed that heating the sample through the T_M is necessary for HI-AOS to take place. Later it was confirmed that heating the sample through T_M is not a necessary condition for HI-AOS [9]. The T_M of $Tb_{20}Co_{80}$ is also below room temperature (300 K), but it shows a deterministic HI-AOS. In the case of $Tb_{34}Co_{66}$, and $Tb_{36}Co_{64}$, the absence of HI-AOS cannot be attributed to the non existence of T_M. Reports on HI-AOS in RE-TM alloys say samples without T_M can also show a deterministic switching. For each composition showing HI-AOS, we have calculated critical fluence values to observe the HI-AOS. Fig. 3 shows the variation of critical fluences with composition. At a lower concentration of Tb, a higher fluence is required to switch the magnetization, and we observe a steady decrease in the value of critical fluence (F_c) as the Tb concentration increases. This decrease in F_c is due to the increase in the number of antiferromagnetic interactions and also due to the reduction of ferromagnetic exchange interaction at the Co sites as Tb concentration increases. To substantiate the role of ferromagnetic exchange interaction at the Co sites in HI-AOS, we reduced the J_{Co-Co}^{eff} by 5% and 10%, respectively, without altering the composition. $Tb_{26}Co_{74}$ shows a 2.1% reduction in F_c value for a 5% decrease in J_{Co-Co}^{eff} and a 10% decrease result in an 8.2% reduction in F_c value. We have repeated this for $Tb_{22}Co_{78}$ and $Tb_{30}Co_{70}$ also and we observe a consistent decrease in F_c values with a reduction in J_{Co-Co}^{eff}. Further, to verify the role of the total number of antiferromagnetic interactions in HI-AOS, we vary the Tb concentration in an interval of 2% by keeping the exchange constants fixed. The Tb composition is varied from 22% to 24% with an increment of 0.5%, and we observe a steady decrease in F_c values as Tb concentration increases, which signifies the role of the total number of antiferromagnetic interactions in HI-AOS in RE-TM alloys.

3.2. Role of element specific damping on HI-AOS in amorphous Tb_xCo_{100-x}

Elucidating the role of phenomenological damping constant in HI-AOS is crucial to understanding and controlling the phenomena of HI-AOS. The phenomenological damping constant couples the spin system to electronic temperature, and it transfers the thermal energy between these subsystems. To comprehend the impact of the damping parameter on HI-AOS, we apply an element specific damping to both Co
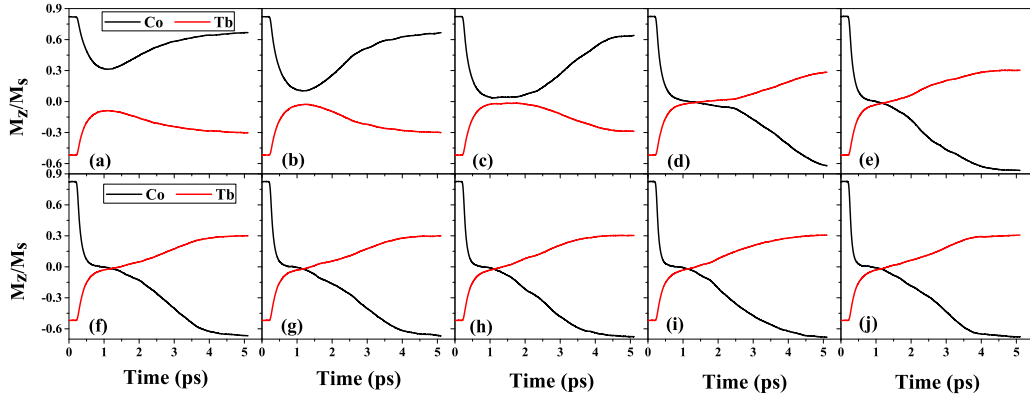
Fig. 4. The element specific magnetization dynamics of $Tb_{26}Co_{74}$ for the different λ_{Co} values at a fixed fluence of 40 mJ/cm^2 and a pulse duration of 50 fs. (a) λ_{Co} = 0.005, (b) λ_{Co} = 0.01, (c) λ_{Co} = 0.015, (d) λ_{Co} = 0.02,(e) λ_{Co} = 0.025, (f) λ_{Co} = 0.03, (g) λ_{Co} = 0.035, (h) λ_{Co} = 0.04, (i) λ_{Co} = 0.045, and (j) λ_{Co} = 0.05. Black and Red lines represent Co and Tb magnetization, respectively.
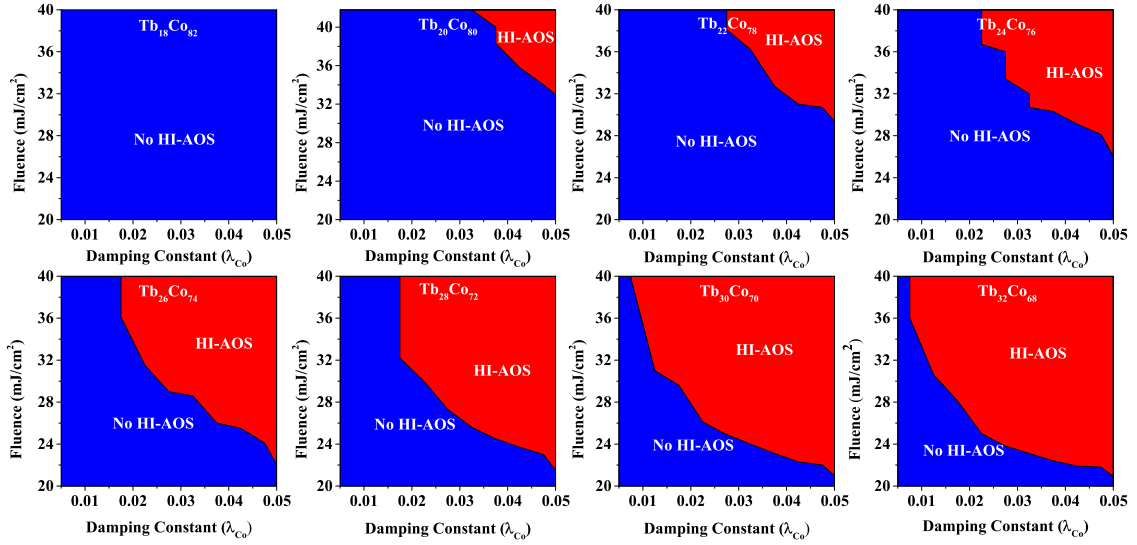

Fig. 5. Switching diagram of Tb_xCo_{100-x} with x = 18 to x = 32 for different λ_{Co} values. The red colour indicates the regions with a deterministic HI-AOS, and blue stands for the region with no HI-AOS.

and Tb sublattices. In the previous section, we assigned equal damping to both sublattices. Here, we kept the damping constant of Tb at 0.05, and that of Co varied from 0.005 to 0.05. Fig. 4 shows the element specific magnetization dynamics of $Tb_{26}Co_{74}$ for the different λ_{Co} values at a fixed fluence of 40 mJ/cm^2 and a pulse duration of 50 fs. The results show that no HI-AOS happens below the value of λ_{Co} = 0.02. For each case showing HI-AOS, we have estimated the threshold energy for HI-AOS to take place. Fig. 5 shows the switching diagram for the different λ_{Co} values at different compositions of Tb_xCo_{100-x}, where x ranges from 18% to 32%. As in the previous case, we do not observe HI-AOS for $Tb_{18}Co_{82}$; for all other compositions, we observe a deterministic switching. Switching occurs at high λ_{Co} values at low Tb concentrations, and it shifts to the lower side as Tb concentration increases. The results show that critical fluence (F_c) values decrease as λ_{Co} increases. As mentioned before, the phenomenological damping constant couples the spin system to the electron temperature (T_e); therefore, an increase in the damping parameter increases electron-spin coupling. The increased electron-spin coupling results in a faster transfer of thermal energy from the electron to the spin system, which enables the stimulation

of magnetization reversal at lower fluences [26,27]. This observation holds true for all compositions within the aforementioned range.

This study summarises the HI-AOS in amorphous TbCo theoretically and defines a range of parameters that can show HI-AOS. To date, there have been no reports on the experimental observation of HI-AOS in amorphous TbCo. But single shot HI-AOS is observed in Tb/Co multilayers having Tb/Co thickness ratio within the range of 1.3–1.5 [21], but the study lacks the time dynamics of the magnetization reversal. A Cebalos et al. [23] studied HI-AOS in $Gd_{22-x}Tb_xCo_{78}$, and HI-AOS is observed up to x = 18%. Only a thermal demagnetization is observed in $Tb_{22}Co_{78}$. S Alebrand et al. [35] investigated HI-AOS in amorphous TbCo for three different compositions, and they observed only a transient magnetization reversal. Here, in our study, we investigated the HI-AOS in amorphous TbCo over a large composition and fluence range. Also, we show the role of damping in HI-AOS. Since the magnetic properties of RE-TM are tunable by controlling their composition and growth conditions, proper engineering of the material system can help to observe HI-AOS in Tb based material. Therefore, the parameter space that we defined here can guide future experiments in this direction.

4. Summary

In conclusion, a theoretical model based on atomistic spin dynamics simulations has been constructed to investigate the laser induced magnetization dynamics in amorphous Tb_xCo_{100-x} alloys. With this model, we performed a series of simulations to investigate the possibility of HI-AOS in Tb_xCo_{100-x} with x ranging from 18 to 36, and hence to find the range of the parameter, it can show HI-AOS. The results show that the HI-AOS is possible in amorphous Tb_xCo_{100-x} alloys for the range of Tb concentration $x = 20$ to $x = 32$ with a 50 fs laser pulse, and only a thermal demagnetization is observed for the compositions $x = 18$, $x = 34$, and $x = 36$. For each composition, we have calculated critical laser fluence at which it shows a deterministic magnetization switching, and it is found that higher laser fluences are required to switch the magnetization at a lower Tb value, and it decreases as Tb concentration increases. We attribute this decrease in F_c to the increase in the number of antiferromagnetic interactions and also to the reduction of ferromagnetic interaction at Co sites as Tb concentration increases.

Further, to understand the role of the damping parameter on HI-AOS, element-specific damping is applied to both sublattices, and the damping parameter of Co is varied from 0.005 to 0.05 while keeping that of Tb at 0.05. Results show that the damping parameter strongly influences HI-AOS, and higher damping values are critical for HI-AOS. At lower λ_{Co} values, higher laser fluences are required to observe HI-AOS, and F_c values decrease as λ_{Co} values increases. This decrease in F_c values with λ_{Co} is valid for all the compositions. The threshold values of λ_{Co} to observe HI-AOS decreases with the increase in Tb concentration. We attribute the decrease in F_c with the increase in λ_{Co} values to the enhanced electron-spin coupling, which speeds up the energy transfer from the electron to the spin system.

CRediT authorship contribution statement

Syam Prasad P.: Conceptualization, Methodology, Investigation, Validation, Software, Formal analysis, Writing – original draft. **Jyoti Ranjan Mohanty:** Conceptualization, Methodology, Writing – review & editing, Resources, Supervision.

Declaration of competing interest

The authors declare that they have no known competing financial interests or personal relationships that could have appeared to influence the work reported in this paper.

Data availability

Data will be made available on request.

Acknowledgements

Appendix A. Supplementary data

Supplementary material related to this article can be found online at https://doi.org/10.1016/j.jmmm.2023.170701.

References

[1] E. Beaurepaire, J.-C. Merle, A. Daunois, J.-Y. Bigot, Ultrafast spin dynamics in ferromagnetic nickel, Phys. Rev. Lett. 76 (22) (1996) 4250, http://dx.doi.org/10.1103/PhysRevLett.76.4250.

[2] J. Hohlfeld, E. Matthias, R. Knorren, K. Bennemann, Nonequilibrium magnetization dynamics of nickel, Phys. Rev. Lett. 78 (25) (1997) 4861, http://dx.doi.org/10.1103/PhysRevLett.78.4861.

[3] J.-Y. Bigot, M. Vomir, E. Beaurepaire, Coherent ultrafast magnetism induced by femtosecond laser pulses, Nat. Phys. 5 (7) (2009) 515–520, http://dx.doi.org/10.1038/nphys1285.

[4] C.D. Stanciu, F. Hansteen, A.V. Kimel, A. Kirilyuk, A. Tsukamoto, A. Itoh, T. Rasing, All-optical magnetic recording with circularly polarized light, Phys. Rev. Lett. 99 (4) (2007) 047601, http://dx.doi.org/10.1103/PhysRevLett.99.047601.

[5] C. Stanciu, A. Kimel, F. Hansteen, A. Tsukamoto, A. Itoh, A. Kirilyuk, T. Rasing, Ultrafast spin dynamics across compensation points in ferrimagnetic GdFeCo: The role of angular momentum compensation, Phys. Rev. B 73 (22) (2006) 220402, http://dx.doi.org/10.1103/PhysRevB.73.220402.

[6] C. Stanciu, A. Tsukamoto, A. Kimel, F. Hansteen, A. Kirilyuk, A. Itoh, T. Rasing, Subpicosecond magnetization reversal across ferrimagnetic compensation points, Phys. Rev. Lett. 99 (21) (2007) 217204, http://dx.doi.org/10.1103/PhysRevLett.99.217204.

[7] A. Kimel, A. Kirilyuk, P. Usachev, R. Pisarev, A. Balbashov, T. Rasing, Ultrafast non-thermal control of magnetization by instantaneous photomagnetic pulses, Nature 435 (7042) (2005) 655–657, http://dx.doi.org/10.1038/nature03564.

[8] S. Alebrand, A. Hassdenteufel, D. Steil, M. Cinchetti, M. Aeschlimann, Interplay of heating and helicity in all-optical magnetization switching, Phys. Rev. B 85 (9) (2012) 092401, http://dx.doi.org/10.1103/PhysRevB.85.092401.

[9] T. Ostler, J. Barker, R. Evans, R. Chantrell, U. Atxitia, O. Chubykalo-Fesenko, S. El Moussaoui, L. Le Guyader, E. Mengotti, L. Heyderman, et al., Ultrafast heating as a sufficient stimulus for magnetization reversal in a ferrimagnet, Nature Commun. 3 (1) (2012) 1–6, http://dx.doi.org/10.1038/ncomms1666.

[10] I. Radu, K. Vahaplar, C. Stamm, T. Kachel, N. Pontius, H. Dürr, T. Ostler, J. Barker, R. Evans, R. Chantrell, et al., Transient ferromagnetic-like state mediating ultrafast reversal of antiferromagnetically coupled spins, Nature 472 (7342) (2011) 205–208, http://dx.doi.org/10.1038/nature09901.

[11] A. El-Ghazaly, B. Tran, A. Ceballos, C.-H. Lambert, A. Pattabi, S. Salahuddin, F. Hellman, J. Bokor, Ultrafast magnetization switching in nanoscale magnetic dots, Appl. Phys. Lett. 114 (23) (2019) 232407, http://dx.doi.org/10.1063/1.5098453.

[12] M. Lalieu, M. Peeters, S. Haenen, R. Lavrijsen, B. Koopmans, Deterministic all-optical switching of synthetic ferrimagnets using single femtosecond laser pulses, Phys. Rev. B 96 (22) (2017) 220411, http://dx.doi.org/10.1103/PhysRevB.96.220411.

[13] J. Gorchon, C.-H. Lambert, Y. Yang, A. Pattabi, R.B. Wilson, S. Salahuddin, J. Bokor, Single shot ultrafast all optical magnetization switching of ferromagnetic Co/Pt multilayers, Appl. Phys. Lett. 111 (4) (2017) 042401, http://dx.doi.org/10.1063/1.4994802.

[14] C. Xu, T. Ostler, R. Chantrell, Thermally induced magnetization switching in Gd/Fe multilayers, Phys. Rev. B 93 (5) (2016) 054302, http://dx.doi.org/10.1103/PhysRevB.93.054302.

[15] U. Atxitia, T.A. Ostler, R.W. Chantrell, O. Chubykalo-Fesenko, Optimal electron, phonon, and magnetic characteristics for low energy thermally induced magnetization switching, Appl. Phys. Lett. 107 (19) (2015) 192402, http://dx.doi.org/10.1063/1.4935416.

[16] R. Moreno, S. Khmelevskyi, O. Chubykalo-Fesenko, Role of exchange parameters for ultrafast thermally induced magnetization switching in ferrimagnets, Phys. Rev. B 99 (18) (2019) 184401, http://dx.doi.org/10.1103/PhysRevB.99.184401.

[17] F. Jakobs, T. Ostler, C.-H. Lambert, Y. Yang, S. Salahuddin, R.B. Wilson, J. Gorchon, J. Bokor, U. Atxitia, Unifying femtosecond and picosecond single-pulse magnetic switching in Gd-Fe-Co, Phys. Rev. B 103 (10) (2021) 104422, http://dx.doi.org/10.1103/PhysRevB.103.104422.

[18] J. Dewhurst, S. Shallcross, I. Radu, P. Elliott, C.v. Korff Schmising, S. Sharma, Ab initio study of ultrafast spin dynamics in Gd x (FeCo) 1- x alloys, Appl. Phys. Lett. 120 (4) (2022) 042401, http://dx.doi.org/10.1063/5.0075057.

[19] S. Mangin, M. Gottwald, C. Lambert, D. Steil, V. Uhlíř, L. Pang, M. Hehn, S. Alebrand, M. Cinchetti, G. Malinowski, et al., Engineered materials for all-optical helicity-dependent magnetic switching, Nature Mater. 13 (3) (2014) 286–292, http://dx.doi.org/10.1038/nmat3864.

[20] S. Alebrand, M. Gottwald, M. Hehn, D. Steil, M. Cinchetti, D. Lacour, E.E. Fullerton, M. Aeschlimann, S. Mangin, Light-induced magnetization reversal of high-anisotropy TbCo alloy films, Appl. Phys. Lett. 101 (16) (2012) 162408, http://dx.doi.org/10.1063/1.4759109.

[21] L. Avilés-Félix, A. Olivier, G. Li, C.S. Davies, L. Álvaro-Gómez, M. Rubio-Roy, S. Auffret, A. Kirilyuk, A. Kimel, T. Rasing, et al., Single-shot all-optical switching of magnetization in Tb/Co multilayer-based electrodes, Sci. Rep. 10 (1) (2020) 1–8, http://dx.doi.org/10.1038/s41598-020-62104-w.

[22] T.-M. Liu, T. Wang, A.H. Reid, M. Savoini, X. Wu, B. Koene, P. Granitzka, C.E. Graves, D.J. Higley, Z. Chen, et al., Nanoscale confinement of all-optical magnetic switching in tbfeco-competition with nanoscale heterogeneity, Nano Lett. 15 (10) (2015) 6862–6868, http://dx.doi.org/10.1021/acs.nanolett.5b02743.

[23] A. Ceballos, A. Pattabi, A. El-Ghazaly, S. Ruta, C.P. Simon, R.F. Evans, T. Ostler, R.W. Chantrell, E. Kennedy, M. Scott, et al., Role of element-specific damping in ultrafast, helicity-independent, all-optical switching dynamics in amorphous (Gd, Tb) Co thin films, Phys. Rev. B 103 (2) (2021) 024438, http://dx.doi.org/10.1103/PhysRevB.103.024438.

[24] R. Moreno, T. Ostler, R. Chantrell, O. Chubykalo-Fesenko, Conditions for thermally induced all-optical switching in ferrimagnetic alloys: Modeling of TbCo, Phys. Rev. B 96 (1) (2017) 014409, http://dx.doi.org/10.1103/PhysRevB.96.014409.

[25] W. Zhang, J.X. Lin, T.X. Huang, G. Malinowski, M. Hehn, Y. Xu, S. Mangin, W. Zhao, Role of spin-lattice coupling in ultrafast demagnetization and all optical helicity-independent single-shot switching in Gd 1- x- y Tb y Co x alloys, Phys. Rev. B 105 (5) (2022) 054410, http://dx.doi.org/10.1103/PhysRevB.105.054410.

[26] N. Kazantseva, U. Nowak, R.W. Chantrell, J. Hohlfeld, A. Rebei, Slow recovery of the magnetisation after a sub-picosecond heat pulse, Europhys. Lett. 81 (2) (2007) 27004, http://dx.doi.org/10.1209/0295-5075/81/27004.

[27] I. Radu, G. Woltersdorf, M. Kiessling, A. Melnikov, U. Bovensiepen, J.-U. Thiele, C.H. Back, Laser-induced magnetization dynamics of lanthanide-doped permalloy thin films, Phys. Rev. Lett. 102 (11) (2009) 117201, http://dx.doi.org/10.1103/PhysRevLett.102.117201.

[28] M. Ellis, T. Ostler, R. Chantrell, Classical spin model of the relaxation dynamics of rare-earth doped permalloy, Phys. Rev. B 86 (17) (2012) 174418, http://dx.doi.org/10.1103/PhysRevB.86.174418.

[29] R.F. Evans, W.J. Fan, P. Chureemart, T.A. Ostler, M.O. Ellis, R.W. Chantrell, Atomistic spin model simulations of magnetic nanomaterials, J. Phys.: Condens. Matter 26 (10) (2014) 103202, http://dx.doi.org/10.1088/0953-8984/26/10/103202.

[30] S. Chadov, J. Minár, M. Katsnelson, H. Ebert, D. Ködderitzsch, A. Lichtenstein, Orbital magnetism in transition metal systems: The role of local correlation effects, Europhys. Lett. 82 (3) (2008) 37001, http://dx.doi.org/10.1209/0295-5075/82/37001.

[31] K. Döbrich, G. Bihlmayer, K. Starke, J. Prieto, K. Rossnagel, H. Koh, E. Rotenberg, S. Blügel, G. Kaindl, Electronic band structure and Fermi surface of ferromagnetic Tb: Experiment and theory, Phys. Rev. B 76 (3) (2007) 035123, http://dx.doi.org/10.1103/PhysRevB.76.035123.

[32] P. Hansen, C. Clausen, G. Much, M. Rosenkranz, K. Witter, Magnetic and magneto-optical properties of rare-earth transition-metal alloys containing Gd, Tb, Fe, Co, J. Appl. Phys. 66 (2) (1989) 756–767, http://dx.doi.org/10.1063/1.343551.

[33] I. Turek, J. Kudrnovský, V. Drchal, P. Bruno, S. Blügel, Ab initio theory of exchange interactions in itinerant magnets, Phys. Status Solidi (B) 236 (2) (2003) 318–324, http://dx.doi.org/10.1002/pssb.200301671.

[34] W. Thoburn, S. Legvold, F. Spedding, Magnetic properties of terbium metal, Phys. Rev. 112 (1) (1958) 56, http://dx.doi.org/10.1103/PhysRev.112.56.

[35] S. Alebrand, U. Bierbrauer, M. Hehn, M. Gottwald, O. Schmitt, D. Steil, E.E. Fullerton, S. Mangin, M. Cinchetti, M. Aeschlimann, Subpicosecond magnetization dynamics in TbCo alloys, Phys. Rev. B 89 (14) (2014) 144404, http://dx.doi.org/10.1103/PhysRevB.89.144404.

[36] M. Mansuripur, M. Ruane, Mean-field analysis of amorphous rare earth-transition metal alloys for thermomagnetic recording, IEEE Trans. Magn. 22 (1) (1986) 33–43, http://dx.doi.org/10.1109/TMAG.1986.1064266.

[37] J.-W. Kim, K.-D. Lee, J.-W. Jeong, S.-C. Shin, Ultrafast spin demagnetization by nonthermal electrons of TbFe alloy film, Appl. Phys. Lett. 94 (19) (2009) 192506, http://dx.doi.org/10.1063/1.3130743.